EUROPHYSICS LETTERS 1 June 2002

Europhys. Lett., **58** (5), pp. 718–724 (2002)

Measurement of the ^{3}He mass diffusion coefficient in superfluid ^{4}He over the 0.45–0.95 K temperature range

S. K. Lamoreaux[1], G. Archibald[2], P. D. Barnes[1], W. T. Buttler[1], D. J. Clark[1], M. D. Cooper[1], M. Espy[1], G. L. Greene[1], R. Golub[3], M. E. Hayden[2], C. Lei[2], L. J. Marek[1], J.-C. Peng[1] and S. Penttila[1]

[1] *University of California, Los Alamos National Laboratory, Physics Division Los Alamos, New Mexico 87545, USA*

[2] *Department of Physics, Simon Fraser University 8888 University Drive, Burnaby, B.C., Canada V5A 1S6*

[3] *Hahn-Meitner Institut - Glienicker Str. 100, D-14109 Berlin, Germany*

(received 8 October 2001; accepted in final form 8 February 2002)

PACS. 67.40.Pm – Transport processes.
PACS. 67.40.Bz – Phenomenology and two-fluid models.
PACS. 67.40.Yv – Impurities and other defects.

Abstract. – We have directly measured the mass diffusion coefficient D of ^{3}He in superfluid ^{4}He at temperatures lower than were previously possible. The experimental technique utilizes scintillation light produced when neutrons react with ^{3}He nuclei, and allows measurement of the ^{3}He density integrated along the trajectory of a well-defined neutron beam. By measuring the change in ^{3}He density near a heater as a function of applied heat current, we are able to infer values for D with 20% accuracy. At temperatures below 0.7 K and for concentrations of order 10^{-4}, we find $D = \left[2.0\,^{+2.4}_{-1.2}\right] T^{-(6.5\mp1.2)}$ cm^2/s, in agreement with a theoretical approximation.

Introduction. – We have developed a new technique for studying the distribution of ^{3}He atoms at low concentrations in superfluid ^{4}He and have applied it to the measurement of the ^{3}He mass diffusion coefficient D at temperatures below 1 K. The most reliable previous experimental determinations of D are based on measurements of thermal conductivity and thermal relaxation, which become exceedingly difficult at temperatures below 1 K [1–3]. We are interested in the magnitude of D near and below 0.5 K, where it is expected to be large [4]. The previous experimental work near 1 K show that D increases very rapidly with decreasing temperature; the temperature dependence of D is predicted to be T^{-7} for $T < 0.6$ K [4].

Theory of the experimental technique. – Our method of measuring D is based on a comparison of the ^{3}He distribution in a cell with and without a source of heat in the liquid. In the treatment below we consider heat flow and ^{3}He concentrations that are sufficiently small so that we can assume the liquid is isothermal. We also ignore the relatively infrequent ^{3}He-^{3}He collisions that do not influence the steady-state ^{3}He atom distribution imposed by the heat flow. This system can be analyzed in terms of the usual macroscopic two-fluid model for liquid ^{4}He below the λ point [5]; these two fluids comprise the superfluid component that carries no entropy, and the normal component that, at sufficiently low temperatures, carries

thermal energy as a pure phonon gas. When a heat source and a heat sink are introduced, the heat flux $\boldsymbol{q}$ associated with the normal component flow is

$$\boldsymbol{q} = \rho s T \boldsymbol{v}_n \,, \tag{1}$$

where ρ is the ^{4}He liquid density, s is the entropy per unit mass, T is the temperature, and $\boldsymbol{v}_n$ is the normal component velocity. The ^{3}He atoms scatter from the phonons and are thus carried along with the normal fluid flow. Consequently, the ^{3}He atoms accumulate at the heat sink. The ^{3}He atoms also scatter from the background phonons that exist when the superfluid ^{4}He is at finite temperature; this scattering tends to randomize the ^{3}He distribution. The net effect is described by the mass diffusion equation, which, for ^{3}He concentrations sufficiently small so that the mass and isotopic concentrations are related by a constant multiplicative factor, can be rewritten in terms of the spatially varying isotopic concentration X as

$$X\boldsymbol{v}_n - D\vec{\nabla}X = 0 \tag{2}$$

and is a good approximation for $X < 10^{-2}$ (see, *e.g.*, §29, eqs. (13) and (14) of [5]). In steady state,

$$\frac{\partial \rho s}{\partial t} = 0 = -\vec{\nabla}\cdot \rho s \boldsymbol{v}_n. \tag{3}$$

We assume ρ and s are spatially uniform under isothermal conditions, in which case $\vec{\nabla}\cdot\boldsymbol{v}_n = 0$. Furthermore, if the flow is laminar, then $\vec{\nabla}\times\boldsymbol{v}_n = 0$, which allows us to write $\boldsymbol{v}_n = \vec{\nabla}\Phi$, where the velocity potential Φ satisfies Laplace's equation, $\nabla^2\Phi = 0$. Substituting this result into eq. (2),

$$X\vec{\nabla}\Phi - D\vec{\nabla}X = 0 \Rightarrow \frac{1}{D}\vec{\nabla}\Phi = \frac{1}{X}\vec{\nabla}X = \vec{\nabla}\log(X), \tag{4}$$

which has the solution

$$X = Ce^{\Phi/D}. \tag{5}$$

The coefficient C, determined by the requirement that the total number of ^{3}He atoms must be constant for a closed system, depends on the total heat input and D. For the case of a point heat source of power P in a large bath (*i.e.*, large enough so that we can ignore boundary conditions),

$$q(r) = \frac{P}{4\pi r^2} \Rightarrow v_n(r) = \frac{q(r)}{\rho s T} \Rightarrow \Phi(r) = -\frac{P}{\rho s T}\frac{1}{4\pi r} = -\frac{\alpha}{4\pi r}\,, \tag{6}$$

where r is the distance from the source, and $\alpha = P/(\rho s T)$. In this case,

$$X(r) = Ce^{-\alpha/4\pi D r} \tag{7}$$

and D can be determined by measuring the spatial extent of the ^{3}He-depleted region as a function of P. Alternatively, D can be inferred if the integrated ^{3}He density along a specific path near the heat source is measured as a function of P. The latter approach serves as the basis of the measurements reported here.

Description of the experiment. – Use of a neutron beam to determine tomographically the distribution of ^{3}He atoms subjected to heat currents in a superfluid-^{4}He-filled cell is described in Appendix C of [4]. For the measurements reported here, we use a variant of this technique; we determine the differential heat on/off effect using a fixed and well-characterized neutron beam. A scale drawing of our apparatus is shown in fig. 1. The 100 cm^3 cell containing superfluid ^{4}He is mounted on the end of a horizontal dilution refrigerator; the OFHC copper

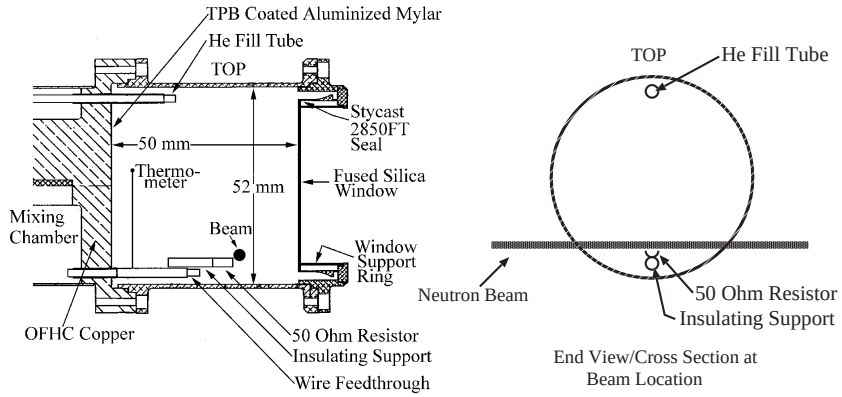

Fig. 1 – Scale drawing of the test cell. There are indium seals at the connections between the aluminum cell cylinder, demountable window, and dilution refrigerator. The cell is filled by condensing the desired mixture of helium isotopes through the fill tube. The 50 Ω resistor serves as the heater.

mixing chamber of the dilution refrigerator, which serves as a heat sink, forms one end of the cell. The cell body is a cylindrical shell of aluminum approximately 1 mm thick. A fused silica window forms the other end of the cell.

Neutrons are absorbed by ^{3}He according to the reaction

$$^3\mathrm{He} + \mathrm{n} \rightarrow \mathrm{p} + \mathrm{t} + 784\ \mathrm{keV} \tag{8}$$

and the energy released to the proton and triton create XUV (80 nm) scintillation light as they are stopped in the superfluid ^{4}He. The XUV light is wavelength-shifted to 450 nm with tetraphenyl butadiene (TPB) evaporated onto the cell walls and onto an aluminized mylar sheet that covers most of the copper end of the cell [6]. The 450 nm light is transmitted through a series of windows. In addition to the cell window, there are two fused silica windows at about 1 K, one fused silica window at about 77 K, an acrylic (blackbody radiation absorbing) window at 77 K, and a fused silica window at room temperature. The scintillations are then detected by a Hamamatsu R329-02 photomultiplier, set to a threshold of 5 ± 0.5 photoelectrons; the detection efficiency of ^{3}He capture events varies spatially within the cell in the 40 to 100% range, with the variation depending primarily on the distance from the mylar sheet.

The experiment was performed at the Los Alamos Neutron Science Center spallation source and used Flight Path 11 A, which comprises a cold neutron guide that views a liquid-hydrogen moderator. The neutron beam was formed by collimating the output of the cold neutron guide to a 2.5 mm FWHM beam with a divergence less than 1×10^{-3} rad. The pulse structure of the source is not crucial to the technique, but was used in our measurements to eliminate the background due to the intense gamma and energetic charged-particle pulse associated with the proton current pulse incident on the spallation target. The pulse counters were gated open in a time window of 6 ms following a delay of 17 ms from the spallation pulse; the distance between the experiment and moderator was 24 m, so the neutron velocity range was 1040 to 1410 m/s. Approximately 3% of the incident neutrons are scattered by the superfluid ^{4}He, and at our level of accuracy, the effects due to scattered incident neutrons can be neglected.

The initial ^{3}He concentration X_0 was varied during the course of the experiment so that between 5 and 20% of the incident neutrons were absorbed, corresponding to $7 \times 10^{-5} \leq X_0 \leq 3 \times 10^{-4}$. The gated count rate was typically 450/s ($X_0 = 10^{-4}$) with a background of 12/s. The background was determined by operating the experiment with the cold neutron

component of the beam blocked by thin Cd and ^{6}Li-doped plastic sheets, and was independent of heat input and relatively insensitive to the ^{3}He concentration. This background was largely due to long-lived molecular optical excitations in the superfluid bath [7] that were left over from the spallation radiation flash. In addition, the neutron beam intensity transmitted through the cell was measured with a ^{6}Li-doped glass scintillator detector, gated identically with the helium scintillation signal. The proton pulse current provided by the facility was used to obtain a relative normalization of the cold neutron intensity.

In order to perform tomography, the cryostat containing the dilution refrigerator and cell was placed on a motor-controlled table that allowed horizontal and vertical motion perpendicular to the neutron beam. Linear resistive displacement transducers linked to the table motion allowed positioning to 0.5 mm absolute accuracy, and to better than 0.25 mm reproducibility. The heat source was a carbon composition resistor (50 Ω at room temperature) located near the bottom of the cell and supported by an insulating alumina column. A calibrated ruthenium oxide temperature-sensing resistor supported by its wire leads was located near the mixing chamber end of the cell as shown in fig. 1. This resistor was used in conjunction with a heater located in the mixing chamber to provide active relative temperature stabilization to within 20 mK under varying heat input conditions. The uncertainty in the absolute temperature was about 0.03 K and depended on the operating temperature. The maximum power delivered to the cell was in the 7 to 15 mW range and was limited by the temperature-dependent cooling power of the refrigerator.

The helium scintillation signal provides a relative measure of the volume-integrated ^{3}He density along the neutron beam. In order to interpret the effects of the applied heat flux it is necessary to determine the velocity potential $\Phi(x, y, z)$ within the cell. This was done by numerically solving $\nabla^2\Phi = 0$ on a $100 \times 100 \times 100$ grid using standard relaxation techniques, with the boundary condition that the perpendicular component of $\boldsymbol{v}_n$ was zero at all boundaries, except at the mixing chamber, where the condition $\Phi = 0$ was set. The perpendicular component of $\boldsymbol{v}_n$ at the resistor surface was determined by the total heat input and assumed to be uniform. Finally, the normalization was determined by integrating e^{Φ} over the grid, with D left as a parameter (scale factor) to be determined experimentally. The integrated ^{3}He density was determined by evaluating the integral of X over the neutron, as the beam shown in fig. 1.

We verified experimentally that eq. (5) does indeed describe the distribution of ^{3}He in the cell subject to heat flow (to be published). For determining D, the beam was directed through the cell in the region near the heater; the beam location used for the measurements is indicated in fig. 1. Results of the numerical calculation of the integrated ^{3}He density along the neutron path shown in fig. 1 are given in fig. 2 as a function of heat power; the value of D at a given temperature enters as an unknown scale factor on the horizontal axis of fig. 2. By measuring the relative rate of change of scintillation rate R (which is proportional to the relative change in integrated ^{3}He density) near zero power, D can be determined from

$$D = \frac{-0.078\ \mathrm{cm}^{-1}}{\mathrm{d}R/\mathrm{d}\alpha}, \tag{9}$$

where the numerical factor is the maximum slope (*i.e.*, at zero heat power) in fig. 2. Because we expect that D scales as T^{-7} at low temperatures (see below), we can cast the data in terms of a universal function if we plot the experimentally observed relative change in scintillation rate as a function of $x = \alpha T^7$. Then eq. (9), with α replaced by x, yields D_T directly, where $D = D_T T^{-7}$.

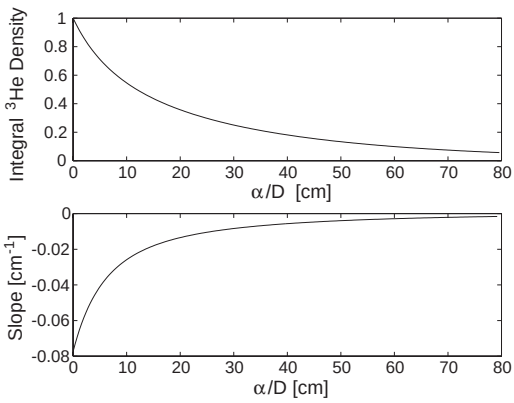

Fig. 2

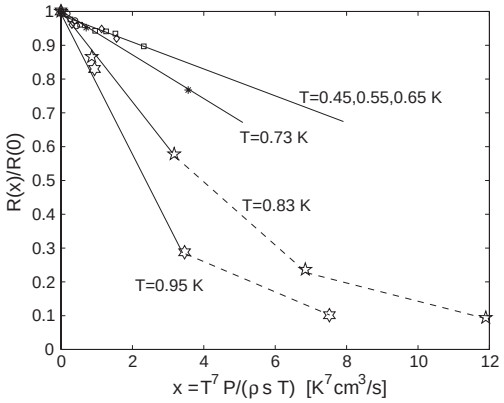

Fig. 3

Fig. 2 – Numerical results for the relative change in the integrated ^{3}He density integrated along the neutron beam path as a function of input power P, parameterized as α/D; the lower plot shows the numerical derivative of the upper plot. These results are specific to the geometry of our experiment.

Fig. 3 – Experimentally determined relative change in scintillation rate data plotted as a function of $x = \alpha T^7$. The data points for $R(x)/R(0) > 0.6$ represent a total count of about 30000 scintillation pulses, from which a background of 1000 has been subtracted; the background is independent of ^{3}He density and heater power. The errors in temperature and relative counting statistics are of order the size of the symbols used to plot the data. The solid lines indicate the slope at low heater power, while the dashed lines indicate the trends in the data at high power.

Experimental results. – The data set is shown in fig. 3. The relative scintillation rate $R(x)/R(0)$ as a function of heater power (parameterized by x) was determined by subtracting the background rate from the observed scintillation rate, and dividing by the background-subtracted scintillation rate at zero power. The vertical errors were determined by counting statistics, while the horizontal errors were determined by the estimated uncertainties in T (and therefore s). The low-temperature points tend to fall on the same curve; the small values of T^7 at the lower temperatures, along with the limited cooling power of the dilution refrigerator, restricted these data to $x \leq 2.2$ as shown in fig. 3. This is sufficiently small so that the variation in relative scintillation rate can be assumed to be linear over the range $0 \leq x \leq 2.2$ (see fig. 2). The low-temperature points (*e.g.*, the data below 0.7 K) are re-plotted in fig. 4 using expanded axes. The points fall on a single line with reduced $\chi^2 = 0.78$. From the slope of this line, along with eq. (9), we arrive at

$$D = D_T T^{-7} = (1.6 \pm 0.2) T^{-7} \quad \mathrm{cm}^2/\mathrm{s}. \tag{10}$$

As expected, there was no observed effect due to concentration (*e.g.*, the low-temperature data are consistent as indicated by χ^2), so we present no analysis on the effect of varying X_0. Also, from eq. (1), $v_n < 10$ cm/s for all the data; this is sufficiently small so that turbulence effects are unlikely to be important.

Finally, D was determined at each temperature independently as shown in fig. 5, along with results from previous work. In this plot, our results clearly indicate a major change in the temperature dependence of D around 0.7 K.

One can further analyze the lowest-temperature data in a two-dimensional fit using $D = D_T T^{-N}$ yielding

$$D = \begin{bmatrix} 2.0 \, {}^{+2.4}_{-1.2} \end{bmatrix} T^{-(6.5 \mp 1.2)} \quad \mathrm{cm}^2/\mathrm{s} \tag{11}$$

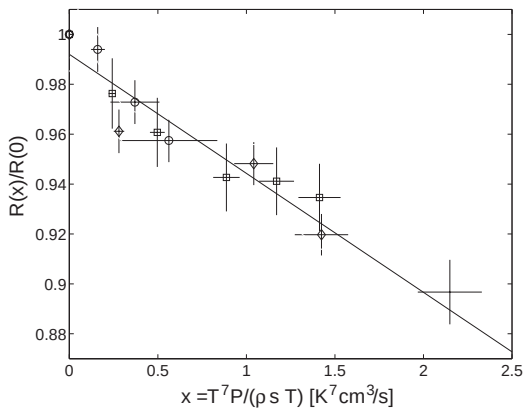

Fig. 4

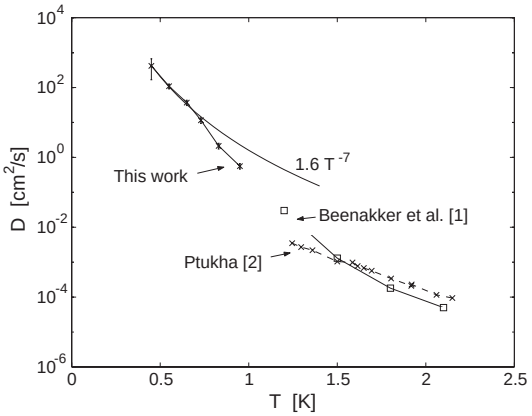

Fig. 5

Fig. 4 – An expanded view of the low-temperature data from fig. 3, which fall on a single line in the low-power regime (circles, 0.45 K; diamonds, 0.55 K; squares, 0.65 K). This behavior indicates that D scales as T^{-7}. A least-squares fit to a line $y = mx + b$ gives $b = 0.992 \pm 0.004$, $m = (-4.77 \pm 0.45) \times 10^{-2}\mathrm{s/cm^3K^7}$, with a reduced $\chi^2 = 0.78$.

Fig. 5 – A comparison of our results for the mass diffusion coefficient D of ^{3}He in superfluid ^{4}He below 1 K with those of previous workers at higher temperatures. The more recent measurements over the 1.38 to 2.18 K temperature range reported in [3], not shown in this plot, agree closely with those of Ptukha [2].

and indicate the level at which the theory presented below is constrained by the experiment.

Microscopic theory of ^{3}He impurity diffusion. – The expectation that D will vary as T^{-7} when collisions with phonons provide the dominant ^{3}He scattering mechanism ($T < 0.6$ K) was briefly discussed in ref. [4] (sect. 7.2); here we add further details to that argument. From fig. 2 of [8] we infer that the ^{3}He-phonon collision frequency $1/\tau_{\mathrm{ph}}$ varies as T^4. The data at $T = 0.5$ K and concentration $X = 1 \times 10^{-3}$ in this figure imply

$$1/\tau_{\mathrm{ph}} = 4.8 \times 10^{10} X T^4 \ \mathrm{s}^{-1}. \tag{12}$$

Because the number of collisions per unit volume per unit time must be the same for phonons and ^{3}He atoms, we have

$$\frac{n_{\mathrm{ph}}}{\tau_{\mathrm{ph}}} = \frac{n_3}{\tau_3} \Rightarrow \frac{1}{\tau_3} = \frac{n_{\mathrm{ph}}}{n_3}\frac{1}{\tau_{\mathrm{ph}}}\,, \tag{13}$$

where $n_3 = 2 \times 10^{22} X \ \mathrm{cm}^{-3}$. The phonon density is approximately (*e.g.*, [5], §16, eq. (28))

$$n_{\mathrm{ph}} = 8\pi\zeta(3)(kT/hc)^3 = 2 \times 10^{19} T^3 \ \mathrm{cm}^{-3}\,, \tag{14}$$

where $\zeta(3) = 1.202$, $c = 2.4 \times 10^4$ cm/s is the phonon phase velocity, k is Boltzmann's constant, and h is Planck's constant; therefore

$$\frac{1}{\tau_3} = 4.8 \times 10^7 T^7 \ \mathrm{s}^{-1}. \tag{15}$$

The collisions measured in ref. [8] are those effective in phonon transport, *i.e.*, those collisions that change the phonon momentum by a significant amount. For elastic collisions, which dominate here, the momentum transfer for a phonon of momentum q scattered through an

angle θ_q (where $\Delta q = 2q \sin\theta_q/2$) is equal to the momentum transfer to a ^{3}He atom with momentum p_3, scattered through an angle θ_3 (where $\Delta p_3 = 2p_3 \sin\theta_3/2$), in a given collision. For each collision,

$$p_3^2(1-\cos\theta_3) = q^2(1-\cos\theta_q) \Rightarrow \langle 1-\cos\theta_3\rangle \approx \langle 1-\cos\theta_q\rangle\langle q^2\rangle/\langle p_3^2\rangle\,, \tag{16}$$

where $\langle ...\rangle$ indicate a thermal average. From elementary considerations, the average squared momenta are

$$\langle q^2\rangle \approx \frac{\langle E_{\rm ph}^2\rangle}{c^2} \approx \frac{10.4(kT)^2}{c^2}, \qquad \langle p_3^2\rangle = 3kTm_3^*\,, \tag{17}$$

where $m_3^* = 2.2m_3$ is the effective ^{3}He mass in superfluid ^{4}He (m_3 is the ^{3}He atomic mass). Numerically, $\langle q^2\rangle/\langle p_3^2\rangle = 7.5\times10^{-2}T$ so for $T < 1$ K, $p_3^2 \gg q^2$ and $\langle\cos\theta_q\rangle \approx 0$. From kinetic theory, the diffusion coefficient is proportional to the product of $1/\langle 1-\cos\theta_3\rangle$ and $\langle v_3\lambda_3\rangle = \tau_3\langle v_3^2\rangle$, where v_3 is the ^{3}He velocity and $\lambda_3 = v_3\tau_3$ is the distance a ^{3}He atom travels between collisions:

$$D = \frac{1}{3}\langle\lambda_3 v_3\rangle/\langle 1-\cos\theta_q\rangle = \frac{1}{3}\langle v_3^2\rangle\tau_3/\langle 1-\cos\theta_q\rangle. \tag{18}$$

We find that

$$D = 1.2T^{-7}\ \mathrm{cm}^2/\mathrm{s} = D_T T^{-7}. \tag{19}$$

The factor D_T is likely correct to within an order of magnitude and is applicable to temperatures near and below 0.6 K, *e.g.*, where the thermodynamic properties of superfluid ^{4}He are dominated by phonons. More importantly, however, this result indicates the functional form of D at low temperature. The value of D_T from eq. (19) is in reasonable agreement with our experimental result, eq. (10). The deviations from the low-temperature T^{-7} behavior of D that are evident for $T > 0.65$ K in fig. 5 are likely due to the influence of rotons at higher temperatures.

Conclusion. – We have employed a novel differential absorption technique to directly determine the mass diffusion coefficient D of ^{3}He in superfluid ^{4}He as a function of temperature, and have verified that D follows the predicted T^{-7} behavior (to within 20% accuracy) for temperatures below 0.7 K. For temperatures at and above 0.7 K, our measurements of D deviate significantly (greater than 30%, with the deviation increasing with temperature) from the low-temperature T^{-7} behavior.

* * *

This work was supported by Los Alamos National Laboratory LDRD under Project Numbers 97041, 98039, and 2001526DR.

REFERENCES

[1] Beenakker J. J. M. *et al.*, *Physica*, **18** (1952) 433.
[2] Ptukha T. P., *Sov. Phys. JETP*, **13** (1961) 1112.
[3] Murphy D. and Meyer H., *J. Low Temp. Phys.*, **107** (1997) 175.
[4] Golub R. and Lamoreaux S. K., *Phys. Rep.*, **237** (1994) 1.
[5] London F., *Superfluids*, Vol. **II** (John Wiley and Sons, New York) 1954.
[6] McKinsey D. N. *et al.*, *Nucl. Instrum. Methods B*, **132** (1997) 351.
[7] McKinsey D. N. *et al.*, *Phys. Rev. A*, **59** (1999) 200.
[8] Husson L. P. J. and De Bruyn Ouboter R., *Physica B*, **122** (1983) 201.